ARTICLE

N-donor Stabilized Tin(II) Cations as Efficient ROP Catalysts for Synthesis of Linear and Star-Shaped PLAs via Activated Monomer Mechanism

Received 00th January 20xx,
Accepted 00th January 20xx

DOI: 10.1039/x0xx00000x

Miroslav Novák,*[a] Jan Turek,*[b] Yaraslava Milasheuskaya,[c] Zdeňka Růžičková,[c] Štěpán Podzimek,[a,d] and Roman Jambor[c]

α-iminopyridine ligands L^1 (2-(CH=N(C_6H_2-2,4,6-Ph_3))C_5H_4N), L^2 (2-(CH=N(C_6H_2-2,4,6-tBu_3))C_5H_4N) and L^3 (1,2-(C_5H_4N-2-CH=N)$_2CH_2CH_2$) differing by the steric demand of the substituent on the imine CH=N group and by a number of donating nitrogen atoms were utilized to initiate a Lewis base mediated ionization of $SnCl_2$ in an effort to prepare ionic tin(II) species [$L^{1\text{-}3}$→SnCl][$SnCl_3$]. The reaction of L^1 and L^2 with $SnCl_2$ led to the formation of neutral adducts [L^1→$SnCl_2$] (**2**) and [L^2→$SnCl_2$] (**3**). The preparation of the desired ionic compounds was achieved by subsequent reactions of **2** and **3** with an equivalent of $SnCl_2$ or $GaCl_3$. In contrast, ligand L^3 containing four donor nitrogen atoms showed the ability to ionize $SnCl_2$ and also $Sn(OTf)_2$ yielding [L^3→SnCl][$SnCl_3$] (**7**) and [L^3→Sn(H_2O)][OTf]$_2$ (**8**). The study has thus revealed that the reaction is dependent on the type of the ligand. Prepared complexes **4** – **8** together with a previously reported [{2-((CH$_3$)C=N(C_6H_3-2,6-iPr_2))-6-CH_3O-C_5H_3N}SnCl][$SnCl_3$] (**1**) were tested as catalysts in the ROP of L-lactide, which could operate via an activated monomer mechanism. Finally, a DFT computational study was performed to evaluate the steric and electronic properties of the ionic tin(II) species **1**, **4** – **8** together with their ability to interact with the L-lactide monomer.

Indroduction

Plastics as materials with very high stability are ideal for many industrial applications, such as building materials, electronic components or packaging materials. However, their chemical stability and resistance toward microbial degradation lead to problems with the accumulation and disposal of the plastic waste, especially in the case of traditional plastics made from petroleum. This problem has helped stimulate a great interest in the so-called biodegradable polymers, which are represented in particular by linear aliphatic polyesters.[1] Poly(lactic acid) (PLA) has a privileged position among biodegradable polyesters, since lactide is produced from the natural sources like starch or sugar *via a* bacterial fermentation of D-glucose.[2] Hence, the whole production of PLA is environmentally friendly. Some applications, especially drug delivery systems or surgical implants, require the use of PLA with a well-defined molecular architecture.[3] The most efficient way for the production of such a well-defined PLA deals with the ring opening polymerization (ROP) of lactide initiated by metal complexes.[4]

Over the last two decades, various charge-neutral discrete complexes of general formula L_nMX_m (L is an ancillary ligand, M is a main-group or transition metal and X is usually an alkyl, amido, alkoxide or halide group) have been used as pre-catalysts for the ROP of lactides.[5] The majority of these complexes are supposed to catalyse the ROP *via* a coordination-insertion mechanism. However, these charge-neutral ROP catalyst systems often exhibit limited activity and productivity. Researchers have thus focused on the employment of discrete cationic complexes of formula $[L_nMX_{m-1}]^+$ $[WCA]^-$, where WCA is a weakly coordinating anion.[5e] It is believed that the positive charge should increase the electrophilic character of the metal center and hence provide a higher affinity towards the heteroatom in monomers. This "Lewis acid activated monomer" should then more easily undergo an attack of the reactive nucleophile and the overall performance of ROP catalysts should be increased.

In industry, but also in academia ($Sn(Oct)_2$) remains the most widely used catalyst for the ROP.[6] $Sn(Oct)_2$ enjoys its popularity due to its low cost, robustness and versatility. On the other hand, it exhibits a relatively low catalytic activity. This disadvantage can be overcome by using discrete tin(II) cations as highly catalytically active alternatives. The literature describes a number of cationic tin(II) complexes, which can be divided into three different categories with a general formula of: $[LSn]^+$ (L = monoanionic ligand), $[D→SnX]^+$ (D = Lewis base, X = halide or pseudohalide) and $[D→Sn]^{2+}$ (Chart 1).[7]

[a] *Institute of Chemistry and Technology of Macromolecular Materials, Faculty of Chemical Technology, University of Pardubice, Studentská 573, 53210 Pardubice, Czech Republic,*
Email: miroslav.novak@upce.cz
[b] *Eenheid Algemene Chemie (ALGC), Vrije Universiteit Brussel, Pleinlaan 2, 1050 Brussels, Belgium.*
[c] *Email:jan.turek@vub.be*
[d] *Department of General and Inorganic Chemistry, Faculty of Chemical Technology, University of Pardubice, Studentská 573, 53210 Pardubice, Czech Republic.*
[e] *Synpo, Ltd., S.K. Neumanna 1316, 53207 Pardubice, Czech Republic*
† Electronic supplementary information (ESI) available. CCDC 2078257-2078259. For ESI and crystallographic data in CIF or other electronic format see DOI: 10.1039/x0xx00000x

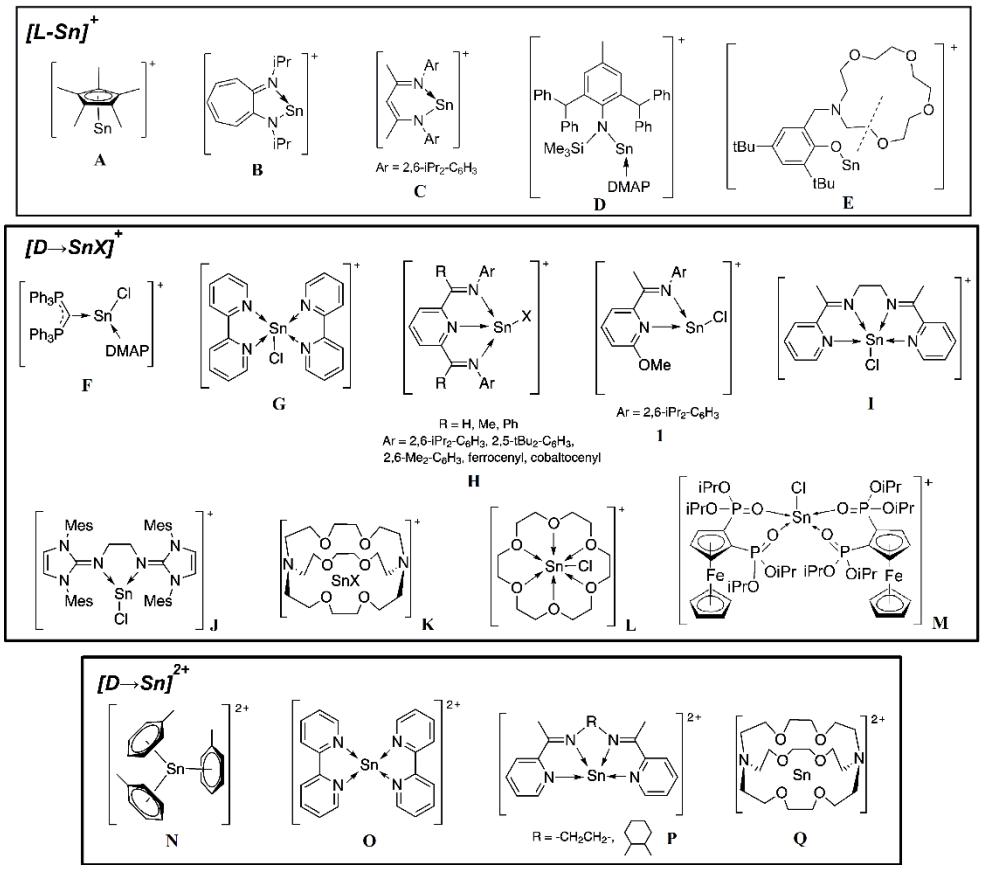

Chart 1 Three different categories of tin(II) cations

Tin(II) cations of $[LSn]^+$ type are stabilized by monoanionic ligands such as permethylated-cyclopentadienyl[8] (**A**), N-isopropyl-2-(isopropylamino)troponimine[9] (**B**), β-diketiminate $CH(CMeNAr)_2^-$ (Ar = 2,6-iPr_2-C_6H_3)[10] (**C**), bulky amido-ligand $\{N(Ar^*)(SiMe_3)\}^-$ (Ar^* = 2,6-$CHPh_2$-4-Me-C_6H_2)[11] (**D**) and amino-ether phenolate LO^{NO4} (2-[(1,4,7,10-tetraoxa-13-azacyclopentadecan-13-yl)methyl]-4,6-di-*tert*-butylphenolate)[12] (**E**). These cations were synthesized predominantly by the dehalogenation of the corresponding halostannylenes. A halide abstraction in $[(Ph_3P)_2C{\cdot}SnCl_2]$ and $[(bipy){\cdot}SnCl_2]$ was also used for the synthesis of $[(Ph_3P)_2C{\cdot}SnCl]_2[AlCl_4]_2$, $[(4\text{-DMAP})(Ph_3P)_2C{\cdot}SnCl][B_{12}Cl_{12}]_{0.5}$ (**F**) and [(bipy)SnCl][OTf] (**G**), representing $[D{\rightarrow}SnX]^+$ cations.[13,14] Roesky et al. observed a Lewis base mediated ionization of $SnCl_2$ and reported the synthesis of $[(DIMPY)SnCl][SnCl_3]$, where DIMPY is 2,6-$[(Me)C{=}N(C_6H_3\text{-}2,6\text{-}iPr_2)]_2C_5H_3N$.[15] In the same manner, we published the stabilization of a tri-coordinated tin(II) cation $[\{2\text{-}((CH_3)C{=}N(C_6H_3\text{-}2,6\text{-}iPr_2))\text{-}6\text{-}CH_3O\text{-}C_5H_3N\}SnCl][SnCl_3]$ (**1**).[16] After that, this synthetic approach has become a powerful tool to obtain a wide range of $[D{\rightarrow}SnX]^+$ cations containing bis(imino)pyridines[17], bis(α-iminopyridines)[18], N-heterocyclic imines[19], cryptands[20], crownether[21] or P-functionalized ferrocene[22] as Lewis bases (**H** – **M**).

After Müller et al. obtained $[(tol)_3Sn]^{2+}$ (**N**) in an attempt to recrystallize stannylium cation in toluene,[23] a significant progress has recently been made in the field of tin(II) dications $[D{\rightarrow}Sn]^{2+}$. The combination of the auto-ionization concept together with the dehalogenation has allowed the synthesis of bipy[14] (**O**) and bis(α-iminopyridine)[18,24] (**P**) stabilized tin(II) dications. An alternative route for the preparation of $[D{\rightarrow}Sn]^{2+}$ is the reaction of cryptands[20] (**Q**) and crown-ethers[21] with tin(II) triflate.

Although the chemistry of tin(II) cations is a relatively well-explored area, only the complex **E**, representing $[L\text{-}Sn]^+$ type of tin (II) cations, was employed as a pre-catalyst in the ROP of cyclic esters. Carpentier and Sarazin reported the ROP of L-lactide (L-LA) catalyzed by the combination of iPrOH with **E** in a molar ratio of [L-LA]:[iPrOH]:[**E**] = 100:10:1.[12] Macromolecular parameters of the isolated PLA exhibited a good control over the polymerization ($M_{n,calc} \approx M_{n,exp}$ = 7000-16100 g/mol, PDI = 1.08-1.3). Based on these findings, it seems that other ionic tin(II) complexes could also be promising pre-catalysts for the ROP of cyclic esters.

As stated, Lewis base mediated ionization is the most powerful method for the synthesis of $[D{\rightarrow}SnX]^+$ cations stabilized by α-iminopyridine ligands. Following the stabilization of the tin(II) cation **1**, we report here the synthesis of a series of tin(II) ionic compounds containing α-iminopyridine ligands $L^{1\text{-}3}$ (L^1 = 2-$(CH{=}N(C_6H_2\text{-}2,4,6\text{-}Ph_3))C_5H_4N$, L^2 = 2-$(CH{=}N(C_6H_2\text{-}2,4,6\text{-}tBu_3))C_5H_4N$ and L^3 = 1,2-$(C_5H_4N\text{-}2\text{-}CH{=}N)_2CH_2CH_2$) (Chart 2).

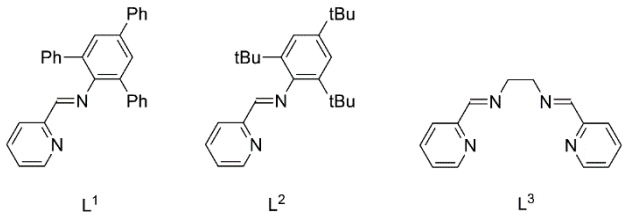

L¹ L² L³

Chart 2 α-iminopyridine ligands L^{1-3} used in this study

Ligands L^{1-3} differ by the steric demand of the substituent on the imine CH=N group (L^1 vs. L^2) and by a number of the donating nitrogen atoms ($L^{1,2}$ vs. L^3), which should affect the electron density on the central tin atom in the discussed tin(II) cations. All complexes together with the earlier reported **1**[16] were then tested as catalyst in the ring-opening polymerization (ROP) of L-lactide for the production of linear PLA. The influence of the steric demand of ligands, coordination number and charge of the central tin atom on the catalytic activity in ROP is also discussed. Selected catalysts were also used for the ROP of L-lactide with the aim to synthesize star-shaped PLA with a dipentaerythritol (DPE) core.

Results and discussion

The treatment of L^1 and L^2 with 1 equiv. of $SnCl_2$ yielded neutral adducts [L^1→$SnCl_2$] (**2**) and [L^2→$SnCl_2$] (**3**) (Scheme 1). This contrasts with the related N-donor ligands,[15-20] which provide the product of the auto-ionization reaction along with the free ligand under the same conditions.

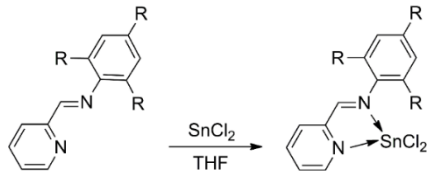

L¹: R = Ph
L²: R = tBu

2: R = Ph
3: R = tBu

Scheme 1 Synthesis of neutral adducts [L^1→$SnCl_2$] (**2**) and [L^2→$SnCl_2$] (**3**)

Compounds **2** and **3** were isolated as an orange powder material characterized by the help of ^{1}H, ^{13}C and ^{119}Sn NMR spectroscopy. The ^{119}Sn NMR spectrum of **2** showed a signal at δ = –227.1 ppm (δ = –219.4 ppm for **3)**, which lies in the range of δ = –161.4 – (–374.8) ppm found in other D→$SnCl_2$ adducts (D = TMEDA, 1-vinylimidazole, 1-benzylimidazole, 1,2,4-triazole).[25,26]

Moreover, the molecular structure of **2** was determined by the single-crystals X-ray diffraction analysis (Figure 1). Suitable single crystals of **2** were obtained from a saturated CH_2Cl_2 solution at room temperature. Crystallographic data of **2** are summarized in Table S1 of the Supporting Information (ESI).

The Sn1 center is tetra-coordinated by N1, N2, Cl1 and Cl2. The N1-Sn1 bond distance (2.3465(18) Å) falls to the region (2.284 – 2.585 Å) typical for N→Sn coordination bonds found in D→$SnCl_2$ adducts (D = TMEDA, 1-vinylimidazole, 1-benzylimidazole, 1,2,4-triazole, bipyridine, phenanthroline).[25-27] On the other hand, the N2-Sn1 bond distance (2.6493(17) Å) is somewhat longer and indicates a weaker donor ability of the imine CH=N group in **2**.

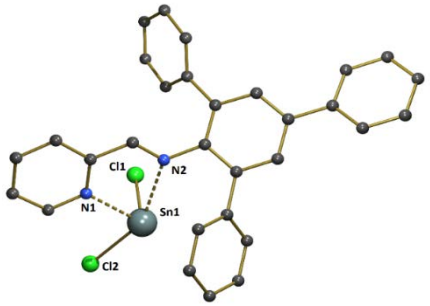

Fig. 1 Molecular structure of **2**. Selected bond distances (Å) and bond angles (°): N1-Sn1 2.3465(18), N2-Sn1 2.6493(17), Sn1-Cl1 2.4685(7), Sn1-Cl2 2.6081(7), N2-Sn1-Cl2 152.63(4), N1-Sn1-N2 66.85(6), Cl1-Sn1-Cl2 88.86(2).

Since the reaction of L^1 and L^2 with $SnCl_2$ led to the formation of neutral compounds **2** and **3**, the preparation of the desired ionic compounds was further studied in subsequent reactions of **2** and **3** with an equivalent of $SnCl_2$ or $GaCl_3$. The experiments revealed that the outcome of these reactions depends on the type of the ligand. While the reaction of **2** with both $SnCl_2$ and $GaCl_3$ led to the isolation of new ionic compounds [L^1→SnCl][$SnCl_3$] (**4**) and [L^1→SnCl][$GaCl_4$] (**5**), compound **3** reacted only with $GaCl_3$ affording [L^2→SnCl][$GaCl_4$] (**6**) (Scheme 2).

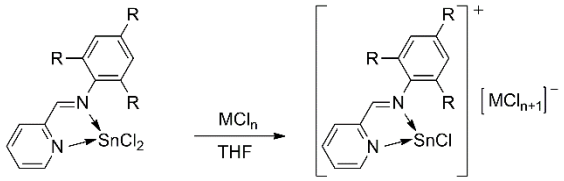

2: R = Ph
3: R = tBu

M = Sn, n = 2
M = Ga, n = 3

4: R = Ph, M = Sn
5: R = Ph, M = Ga
6: R = tBu, M = Ga

Scheme 2 Synthesis of ionic compounds [L^1→SnCl][$SnCl_3$] (**4**), [L^1→SnCl][$GaCl_4$] (**5**) and [L^2→SnCl][$GaCl_4$] (**6**)

Compounds **4** – **6** were isolated as an orange powder material characterized by the help of ^{1}H, ^{13}C and ^{119}Sn NMR spectroscopy along with the MALDI-Orbitrap mass spectrometry. The *ortho*-hydrogen atom of the pyridine ring ($H^{o\text{-}py}$) resonates as a doublet at δ = 9.30 ppm in the ^{1}H NMR spectrum of **4** (δ = 8.84 ppm for **5** and δ = 8.98 ppm for **6**). A singlet at δ = 8.33 ppm was assigned to the imine C*H*=N proton in **4** (δ = 8.47 ppm for **5** and δ = 8.44 ppm for **6**). All these signals are downfield shifted compared to the starting neutral complexes **2** and **3** and support the electrophilic nature of the tin(II) cationic center in **4** – **6**. A ^{119}Sn NMR spectrum at room temperature of a solution of **4** in THF-d8 revealed a single resonance at δ = –235.4 ppm. At –50 °C, this resonance de-coalesced into two equally intense resonances at δ = –254.9 and –347.6 ppm, respectively, as expected for **4**. Apparently, there is an exchange process between the two tin centers, which is fast on the ^{119}Sn NMR time scale at room temperature but slow at low temperature. However, this was not further investigated in detail. In the ^{119}Sn NMR spectra of **5** and **6**, [L^1→SnCl]$^+$ and [L^2→SnCl]$^+$ cations resonate at

δ = –235.5 ppm (for **5**) and δ = –224.4 ppm (for **6**). The signals of $[L^{1,2}\rightarrow SnCl]^+$ are significantly downfield-shifted in comparison to those of the chlorostannyliumylidenes stabilized by the tridentate bis(imino)pyridine ligands (range of –482.4 to –411.7 ppm)[15,17] but are in accordance with the related complex stabilized by a bidentate bis(N-heterocyclic imine) ligand (–240.4 ppm)[19].

The composition of compounds **4** – **6** was further determined by the MALDI-Orbitrap mass spectroscopy. Mass spectra of **4** and **5** displayed a molecular cation $[L^1\rightarrow SnCl]^+$ with m/z = 565.04 and a molecular anion $[SnCl_3]^-$ with m/z = 226.80 ($[GaCl_4]^-$ with m/z = 210.79 for **5**). Similarly, a molecular cation $[L^2\rightarrow SnCl]^+$ with m/z = 505.14 and a molecular anion $[GaCl_4]^-$ with m/z = 210.79 were found in the mass spectrum of **6**.

In contrast to L^1 and L^2, ligand L^3 containing four donor nitrogen atoms showed the ability to autoionize $SnCl_2$. The treatment of L^3 with 1 equiv. of $SnCl_2$ provided $[L^3\rightarrow SnCl][SnCl_3]$ (**7**) and the free ligand, so 2 equiv. of $SnCl_2$ are necessary for a quantitative reaction (Scheme 3). A strong donor ability of L^3 encouraged us to prepare an analogous dicationic tin(II) complex. The reaction of L^3 with $Sn(OTf)_2$ afforded $[L^3\rightarrow Sn(H_2O)][OTf]_2\cdot THF$ (**8**) as an example of $[D\rightarrow Sn]^{2+}$ tin(II) cation (Scheme 3).

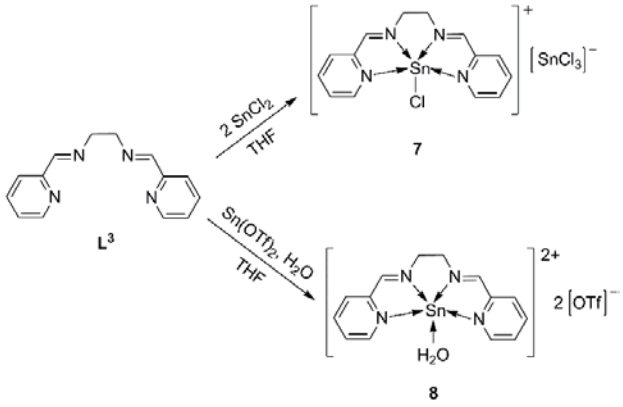

Scheme 3 Synthesis of ionic compounds $[L^3\rightarrow SnCl][SnCl_3]$ (**7**) and $[L^3\rightarrow Sn(H_2O)][OTf]_2$ (**8**)

Compounds **7** and **8** were isolated as an orange (**7**) and a pale yellow (**8**) powder material characterized by the help of ^1H, ^{13}C and ^{119}Sn NMR spectroscopy. A singlet at δ = 9.02 ppm was assigned to the imine C*H*=N proton in **7** (δ = 9.08 ppm for **8**). The ^{119}Sn NMR spectrum of **7** revealed two signals indicating the presence of two non-equivalent tin nuclei. The signal at δ = –592.6 ppm is comparable to that found in [{1,2-(C_5H_4N-2-$C(CH_3)$=N)$_2CH_2CH_2$}SnCl][OTf] (δ = –572.4 ppm)[18] and corresponds to $[L^3\rightarrow SnCl]^+$ cation, while the signal at δ = –25.5 ppm was assigned to $[SnCl_3]^-$ anion. Similarly, the signal found in ^{119}Sn NMR spectrum of **8** (δ = –658.0 ppm) is comparable with signals found in [{1,2-(C_5H_4N-2-$C(CH_3)$=N)$_2CH_2CH_2$}Sn][OTf]$_2$ (δ = –637 ppm)[18] and [{1,2-(C_5H_4N-2-$C(CH_3)$=N)$_2C_6H_{10}$}Sn][OTf]$_2$ (δ = –596 ppm)[24].

Molecular structures of **7** and **8** were unambiguously established by the single-crystals X-ray diffraction analysis (Figures 2 and 3). Suitable single crystals of **7** were obtained from a saturated acetonitrile-hexane solution (THF-acetonitrile for **8**) at –20 °C . Crystallographic data of **7** and **8** are summarized in Tables S2 and S3 (ESI).

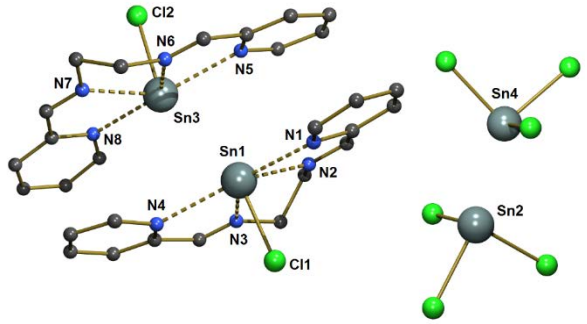

Fig. 2 Molecular structure of **7**. Selected bond distances (Å) and bond angles (°): N1-Sn1 2.631(3), N2-Sn1 2.377(3), N3-Sn1 2.406(3), N4-Sn1 2.627(3), N5-Sn1 2.612(3), N6-Sn1 2.396(3), N7-Sn1 2.382(3), N8-Sn1 2.649(3), Sn1-Cl1 2.4741(12), Sn1-Cl2 2.4794(12), N1-Sn1-N2 68.92(10), N2-Sn1-N3 127.30(10), N1-Sn1-N3 63.95(11), N3-Sn1-N4 151.45(11), N1-Sn1-O1 87.16(10), N3-Sn1-O1 76.60(11).

The molecular structure of **7** reveals the presence of two units, each representing an ionic pair consisting of $[L^3\rightarrow SnCl]^+$ cation compensated by $SnCl_3^-$ anion. The Sn1 (Sn3) center is penta-coordinated by N1-N4 (N5-N8) and Cl1 (Cl2). The coordination arrangement of the central tin atom is closer to a square pyramid than to a trigonal bipyramid with τ = 0.45 (0.43). The tin atom is 0.152 Å (0.168 Å) above the slightly distorted basal plane formed by the four nitrogen atoms. The (pyridine)nitrogen-tin bond distances with the range of 2.612(3) – 2.649(3) Å are longer than the (imino)nitrogen-tin bond distances (range of 2.377(3) - 2.406(3) Å). This is in agreement with N-Sn bond distances found in the recently published [{1,2-(C_5H_4N-2-$C(CH_3)$=N)$_2CH_2CH_2$}SnCl][$SnCl_3$], where N^{py}-Sn are 2.388 and 2.404 Å, while 2.578 and 2.579 Å were established for N^{im}-Sn.[18] A remarkable aspect in the structure of **7** is a secondary intermolecular Sn(1)···Sn(3) interaction of 3.760 Å, that is shorter than twice the van der Waals radius of tin (4.34 Å)[28]. A similar interaction (range of 3.595 – 3.887 Å) was observed in tin(II) bromide, iodide, selenido- and telluridophenolates bearing *O*,*C*,*O*-pincer type of ligand.[29] However, compound **7** is the first example of tin(II) cation revealing such a Sn···Sn interaction.

The molecular structure of **8** consists of $[L^3\rightarrow Sn(H_2O)]^{2+}$ dication and two triflate anions. The Sn1 center is penta-coordinated by N1-N4 and O1. The coordination neighbourhood of the central tin atom can be described as a distorted square pyramid with τ = 0.29. All four nitrogen atoms are almost coplanar and the tin atom is located 0.462 Å above the basal plane. The (pyridine)nitrogen-tin bond distances (N3-Sn1 = 2.702(4) Å and N4-Sn1 = 2.668(3) Å) are longer than the (imino)nitrogen-tin bond distances (N1-Sn1 = 2.400(3) Å and N2-Sn1 = 2.370(3) Å). This elongation is more significant than in the recently published [{1,2-(C_5H_4N-2-$C(CH_3)$=N)$_2CH_2CH_2$}Sn][OTf]$_2$ and [{1,2-(C_5H_4N-2-$C(CH_3)$=N)$_2C_6H_{10}$}Sn][OTf]$_2$, where a range of 2.345 – 2.375 Å was found for N^{py}-Sn and 2.282 – 2.343 Å for N^{im}-Sn.[18,24] The two triflate anions are completely separated from the coordination sphere of tin atom with the shortest oxygen-tin bond distance Sn1-O5 of 4.271(4) Å (cf. $\sum_{vdW}$(Sn,O) = 3.69 Å).[28]

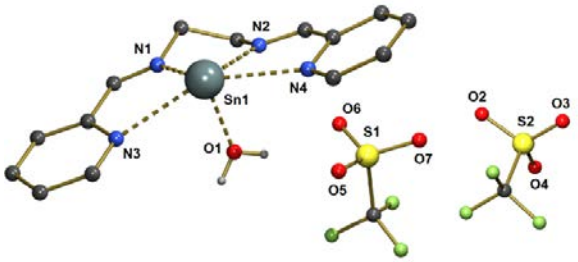

Fig. 3 Molecular structure of **8**. THF molecule is omitted for clarity. Selected bond distances (Å) and bond angles (°): N1-Sn1 2.400(3), N2-Sn1 2.370(3), N3-Sn1 2.702(4), N4-Sn1 2.668(3), Sn1-O1 2.195(3), Sn1-O2 10.567(5), Sn1-O3 11.652(4), Sn1-O4 12.575(4), Sn1-O5 4.271(4), Sn1-O6 4.885(4), Sn1-O7 6.068(4), N1-Sn1-N2 68.92(10), N2-Sn1-N3 127.30(10), N1-Sn1-N3 63.95(11), N3-Sn1-N4 151.45(11), N1-Sn1-O1 87.16(10), N3-Sn1-O1 76.60(11).

A DFT computational study was carried out in order to gain more insight on the formation of the studied complexes and their steric and electronic properties. All geometries were fully optimized at the B3LYP-D3BJ[30]/cc-pVDZ(-PP)[31] level of theory, showing good agreement between the experimental X-ray diffraction data and the calculated structural parameters. The formation of both neutral adducts **2** and **3** is exergonic (ΔG = –18.3 and –16.3 kcal mol^{-1}) and results in very similar structures (Table 1; for optimized geometries of all complexes along with the corresponding Gibbs free energy differences for their formation see Figure S1 and Table S4, ESI). The difference in the strength of the interaction between the central Sn atom and the two different N-donor groups is clearly reflected by the computed Wiberg bond index (WBI)[32] revealing notably higher $WBI_{N\text{-}Sn}$ values for the pyridine group (*ca.* 0.19) than for the imine group (*ca.* 0.08), see Table 2.

Table 1 Gibbs free energy differences (ΔG; in kcal mol^{-1}) for the formation of the studied complexes **2** – **8**.

	ΔG(DZ)[a]	ΔG(TZ)[b]	ΔG^{solv}(TZ)[c]
$L^1 + SnCl_2 \rightarrow$ **2**	–24.6	–20.8	**–18.3**
$L^2 + SnCl_2 \rightarrow$ **3**	–19.8	–17.2	**–16.3**
2 + $SnCl_2 \rightarrow$ **4**	57.4	56.3	**-3.9**
2 + $GaCl_3 \rightarrow$ **5**	41.4	41.0	**–19.9**
3 + $SnCl_2 \rightarrow [L^2SnCl_2][SnCl_3]$	68.4	67.3	**2.4**
3 + $GaCl_3 \rightarrow$ **6**	52.3	52.0	**–13.6**
$L^3 + 2\ SnCl_2 \rightarrow$ **7**	15.3	20.4	**–38.1**
$L^3 + Sn(OTf)_2 + H_2O \rightarrow$ **8**	202.7	187.5	**–15.0**

[a]Calculated at the B3LYP-D3BJ/cc-pVDZ-PP level of theory; [b]calculated at the B3LYP-D3BJ/cc-pVTZ-PP level of theory; [c]calculated at the B3LYP-D3BJ/cc-pVTZ-PP level of theory in THF.

In line with the experimental results, the subsequent reaction with a second equivalent of $SnCl_2$ yielding ionic compounds $[L^{1,2}\rightarrow SnCl][SnCl_3]$ is energetically favourable only for the complex **2** (ΔG = –3.9 and 2.4 kcal mol^{-1} for **4** and $[L^2\rightarrow SnCl][SnCl_3]$). On the other hand, the formation of both ionic compounds **5** and **6** through the reaction with $GaCl_3$ is highly exergonic (ΔG = –19.9 and –13.6 kcal mol^{-1} for **5** and **6**). In contrast to ligands $L^{1,2}$, the ability of the ligand L^3 to autoionize $SnCl_2$ results in a spontaneous formation of the ionic compound **7** (ΔG = –38.1 kcal mol^{-1}), see Table 1.

Table 2 Selected bond lengths (d; in Å), Wiberg bond indices (WBI), and NPA atomic charges (q; in e) for all neutral and cationic complexes **1** – **8**.

	$d_{Sn\text{-}N(Im)}$	$WBI_{Sn\text{-}N(Im)}$	$d_{Sn\text{-}N(Py)}$	$WBI_{Sn\text{-}N(Py)}$	q_{Sn}
2	2.843	0.085	2.536	0.194	1.18
3	2.965	0.070	2.550	0.188	1.15
$\mathbf{1}^+$	2.347	0.265	2.346	0.264	1.25
$\mathbf{4}^+/\mathbf{5}^+$	2.403	0.237	2.418	0.221	1.28
$\mathbf{6}^+$	2.346	0.275	2.393	0.247	1.26
$\mathbf{7}^+$	2.490 2.497	0.216 0.215	2.740 2.758	0.123 0.119	1.21
$\mathbf{8}^{2+}$	2.394 2.423	0.252 0.253	2.695 2.727	0.155 0.139	1.42

As a result of the formation of the ionic complexes **4** – **6** (Figure 4), the N→Sn donor-acceptor interactions become significantly stronger with an average bond length of 2.39 Å and a $WBI_{N\text{-}Sn}$ value of 0.25 for both the pyridine and imine groups (Table 2; for a complete set of selected bond lengths, WBI and NPA atomic charges see Table S5, ESI). Correspondingly, this change in bonding leads to only a marginal increase of the natural population analysis (NPA)[33] charge (*ca*. 0.1 *e*) on the Sn center in comparison to the neutral complexes **2** and **3**. Unlike for **2** - **6**, the imine groups were shown to be stronger donors than the pyridine groups in case of **7** with a tetradentate ligand L^3 (Figure 4).

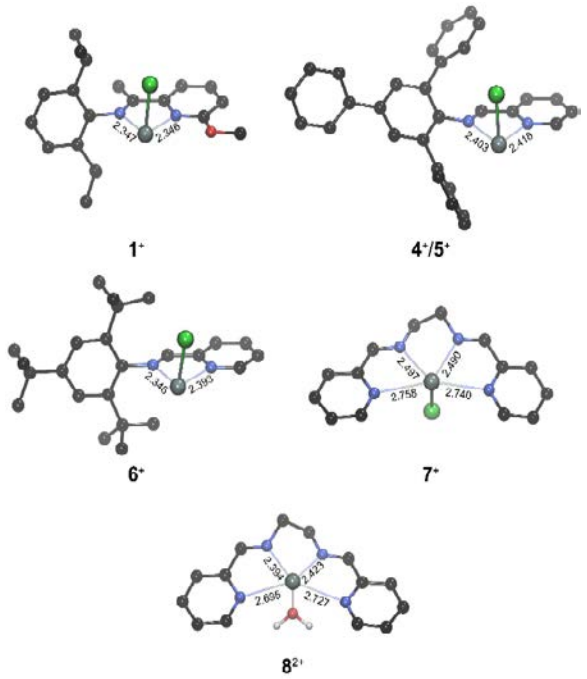

Fig. 4 Optimized geometries of the cationic part of the complexes **1** and **4** - **8** along with selected bond distances (in Å). Hydrogen atoms are omitted for clarity.

The structural parameters found for **7** (Table 2) are comparable with those reported by Majumdar and Raut for a similar compound $[\{1,2\text{-}(C_5H_4N\text{-}2\text{-}C(CH_3)=N)_2CH_2CH_2\}SnCl][SnCl_3]$.[18] The molecular structure of an aqua complex **8** resembles the structure of **7**, where the Cl ligand is replaced by the O atom of H_2O.

Next, the different steric properties of ligands $L^{1,2,3}$ and 2-((CH$_3$)C=N(C$_6$H$_3$-2,6-iPr$_2$))-6-CH$_3$O-C$_5$H$_3$N in the cationic complexes [L→SnCl]$^+$ were investigated using the percentage of buried volume (%V$_{Bur}$)[34] descriptor and visualized using the topographic steric maps.[35] Figure 5 shows that ligand L^1 is the bulkiest among the tridentate ligands with a %V$_{Bur}$ of 45.7%, which is comparable with the value of 44.0% found for the tetradentate ligand L^3. Furthermore, a detailed analysis of the steric maps indicates that the larger steric hindrance in the south-western quadrant might affect the catalytic activity of compound **6** in comparison to **1**, despite almost identical %V$_{Bur}$ values.

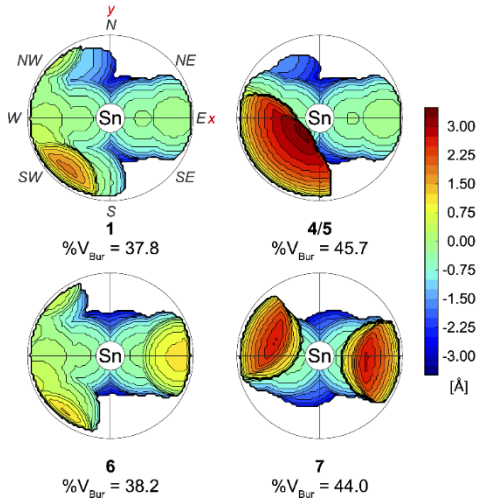

Fig. 5 Topographic steric maps of the ligand L in the cationic complexes **1** and **4** - **7** along with percentage of buried volume values (%V$_{Bur}$).

Beside the steric properties of a ligand, electronic properties should also be considered with respect to the catalytic activity of the studied complexes. Accordingly, the interaction energies between the ligand and the metal centre were evaluated and decomposed using the Ziegler-Rauk energy decomposition analysis (EDA),[36] which allows for the assessment of the relative weights of electrostatic and orbital interactions along with the role of the dispersion interactions (Table 3; for EDA of all complexes **1** – **8** see Table S6, ESI). As expected, the magnitude of the interaction energy (ΔE_{int}) correlates well with the structural data, showing an almost threefold increase of ΔE_{int} for **4**/**5** and **6** compared to **2** and **3**. The largest ΔE_{int} value of –216.3 kcal mol^{-1} was found for the dicationic complex **8**, which is almost twice as big as the value determined for the corresponding monocationic analogue **7** (–119.9 kcal mol^{-1}). In all studied cationic complexes, electrostatic interactions (*ca.* 53 %) are slightly preferred over orbital interactions (*ca.* 41 %) along with a small contribution of dispersion (*ca.* 6 %).

Table 3 Energy decomposition analysis (EDA) for neutral and cationic complexes **1** – **8** (All energies are in kcal mol^{-1}).[a]

	ΔE_{int}	ΔE_{Pauli}	ΔE_{oi}	ΔV_{elstat}	E_{disp}
2	–35.8	89.4	–39.1 (31)	–69.9 (56)	–16.2 (13)
3	–29.0	78.2	–33.6 (31)	–59.2 (55)	–14.4 (13)
1$^+$	–96.2	155.2	–101.6 (40)	–135.3 (54)	–14.4 (6)
4$^+$/**5**$^+$	–97.3	141.7	–99.1 (41)	–123.6 (52)	–16.3 (7)
6$^+$	–87.0	151.0	–99.5 (42)	–123.9 (52)	–14.5 (6)
7$^+$	–119.9	139.6	–97.4 (38)	–147.7 (57)	–14.4 (6)
8^{2+}	–216.3	147.5	–159.1 (44)	–191.2 (53)	–13.5 (4)

[a]Values written in parentheses represent the relative contribution (in %) of the orbital interaction energy, the electrostatic energy, and the dispersion energy with respect to the total stabilization component of the interaction energy.

ROP of L-lactide

Ionic complexes **4** – **8**, together with the earlier reported **1**, were prepared in order to be tested as catalysts in the ROP of L-LA via an activated monomer mechanism (Scheme 4).

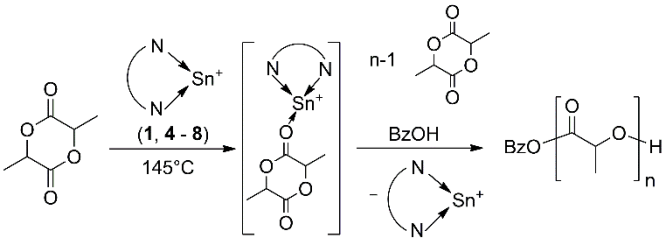

Scheme 4 ROP of lactide catalysed by **1**, **4** - **8**

Due to the differences in the structure of the prepared ionic tin(II) compounds **4** – **6**, the effect of the steric demand of ligands L^1 and L^2 can be studied in the ROP of L-lactide. While the tin(II) atom is tri-coordinated in **4** - **6**, complexes **7** and **8** contain penta-coordinated tin(II) atom. It is thus possible to study the effect of the coordination number of the central tin atom. Furthermore, the effect of the imine CH=N vs. ketimine (CH$_3$)C=N functional group on the catalytic activity of complexes **4** and **1** can also be observed, since both compounds possess identically tri-coordinated central tin atom.

L-LA was once recrystallized to avoid data fluctuations due to the variation of impurities in the technical grade L-LA. All polymerization tests were performed solvent free in melt at 145 °C. The polymerization reactions were carried out in a molar ratio of [catalyst]:[L-LA] = 1:100 and benzyl alcohol (BzOH) was added as a co-initiator in a molar ratio of 1:1 with respect to the catalyst. The conversion of the polymerization experiments was monitored by the ^{1}H NMR spectroscopy and used for the determination of the polymerization rates from the slope of the plot of ln(L-LA$_0$/L-LA$_t$) versus time (min). The polymerization kinetics experiments were performed with complexes **1**, **4**, **7** and **8** and are shown in Figure 6.

Table 4 ROP of L-lactide catalysed by **1**, **4** – **8**.

entry	catalyst	T [°C]	initiator	[cat]:[BzOH]:[LA]	time [min]	conv [%][a]	$M_{n,th}$ [g/mol][b]	$M_{n,SEC}$ [g/mol][c]	*Đ*
1	**1**	145	BzOH	1:1:100	50	100	14500	9900	1.45
2	**4**	145	BzOH	1:1:100	90	96	13950	4000	1.23
3	**5**	145	BzOH	1:1:100	90	94	13650	4012	1.31
4	**6**	145	BzOH	1:1:100	90	90	13100	4600	1.39
5	**7**	145	BzOH	1:1:100	60	94	13600	7800	1.25
6	**8**	145	BzOH	1:1:100	60	95	13800	5600	1.34
7	$Sn(Oct)_2$	145	BzOH	1:1:100	30	99	14400	7200	2.04

[a]measured by the ^1H NMR spectroscopy; [b]calculated M_n of PLA (g/mol): [L-LA]:[cat] · conv · M(L-LA) + M(BzOH); [c]experimental M_n values were determined by SEC analysis in THF solution using polystyrene standards and corrected by a factor of 0.58[37]

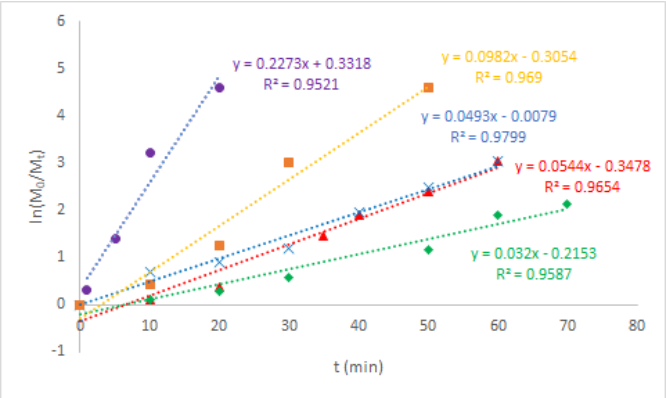

Fig. 6 Plot of $ln[L\text{-}LA]_0/[L\text{-}LA]_t$ versus time using **1** (■), **4** (◆), **7** (▲), **8** (X) and $Sn(Oct)_2$ (●) as catalyst.

For all tested complexes a linear dependence of $ln(L\text{-}LA_0/L\text{-}LA_t)$ versus time was found, indicating a pseudo-first order reaction, and thus a good control over the polymerization proceeding through an activated monomer mechanism. The fastest polymerization rate was observed for complex **1** ($k = 9.82 \cdot 10^{-2}\ min^{-1}$). Polymerizations with **7** and **8** are slower ($k = 5.44 \cdot 10^{-2}\ min^{-1}$ and $4.93 \cdot 10^{-2}\ min^{-1}$ for **7** and **8**), while the slowest polymerization was achieved using complex **4** ($k = 3.2 \cdot 10^{-2}\ min^{-1}$). The test proved a strong influence of the ligand on the polymerization. The comparison of the tri-coordinated tin(II) cations **1** vs. **4** showed a positive electronic effect of a ketimine (Me)C=N group in **1** compared with an imine CH=N in **4** on polymerization rate. In addition, **4** contains more sterically demanding aryl substituent on the nitrogen atom of the CH=N group, which blocks the access of L-LA to the reaction centre and thus the polymerization is slower. The polymerizations with **7** and **8** lie between values achieved by **1** and **4** and indicate that there is no exact dependence of the polymerization rates on the coordination number of the central tin atom in **1**, **4**, **7** and **8**. Moreover, the different charge of the tin atom in **7** and **8** does not affect the polymerization rate.

All isolated polylactides were further characterized by the help of the size exclusion chromatography (SEC) with the aim to determine the number-average molar mass (M_n) and dispersity (*Đ*). Results of the polymerization tests are summarized in Table 4.

It can be seen that despite the different structure of **4** – **6**, these catalysts produce polymers with very similar macromolecular parameters; M_n = 4000 – 4600 g/mol and *Đ* = 1.23 – 1.39 (entry 2 – 4). While *Đ* demonstrates a relatively uniform nature of PLAs, M_n values are lower than the calculated theoretical ones. From these results, it is evident that the different steric hindrance of L^1 and L^2 in **5** and **6** does not affect the macromolecular properties of the prepared PLAs. PLAs with higher M_n values and narrow *Đ* were obtained by using **7** (M_n = 7800 g/mol) and **8** (M_n = 5600 g/mol) as catalysts (entry 5 and 6). The best result was observed for the complex **1** (entry 1), which produces PLA with the highest M_n (9900 g/mol), which is closest to the theoretical M_n.

In addition, TG-GCMS was conducted to determine the end-group of PLA prepared using **1**. The presence of benzyl chloride was detected, which is a clear evidence of the incorporation of a benzyl group into PLA (see Figure S3, ESI).

To compare the catalytic activity of the studied complexes in ROP of L-LA, analogous polymerization tests were performed with a commonly used $Sn(Oct)_2$. Although the rate of the polymerization using $Sn(Oct)_2$ is faster ($k = 22.73 \cdot 10^{-2}\ min^{-1}$), the dispersity (*Đ* = 2.04) of PLA is broader with almost the same M_n (7200 g/mol; entry 7, Table 4).

A good control over the polymerization proceeding via an activated monomer mechanism encouraged us to cleave the activated monomer also using polyalcohol to produce star-shaped PLAs. For these experiments, complexes **1**, **7** and **8** were selected as catalysts. The polymerization conditions were similar to the preparation of linear polymers, except that dipentaerythritol (DPE) was used instead of benzyl alcohol (Scheme 5).

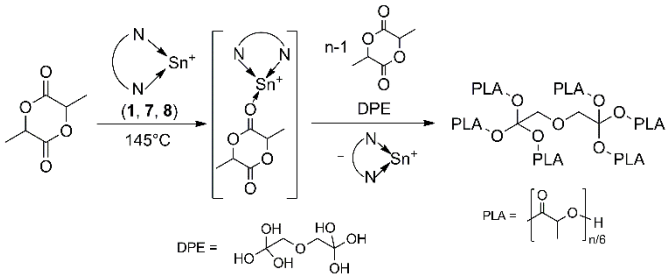

Scheme 5 Synthesis of star-shaped PLAs using **1**, **7** and **8** as catalysts.

The molar mass distribution and branching were characterized by the size exclusion chromatography (SEC) combined with a multi-angle light scattering detector (MALS) and an online viscometer (Visco). The number-average molar mass (M_n), the weight-average molar mass (M_w), the dispersity (M_w/M_n), and the weight-average intrinsic viscosity ($[\eta]_w$) of samples Star 1, Star 2, and Star 3 are listed in Table 5; and their intrinsic viscosities are compared with those of linear PLAs in Figure 7.

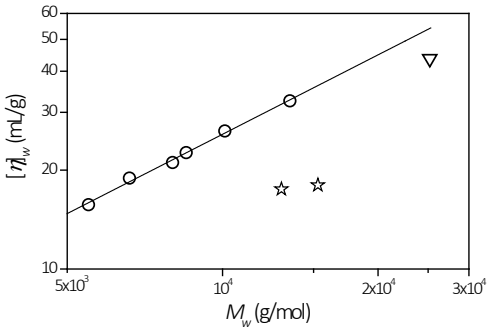

Fig. 7 The plots of $[\eta]_w$ versus M_w for linear PLA (○), Stars 1 and 2 (★), and Star 3 (▽).

Table 5 Molecular characteristics of star-shaped PLAs.

sample	catalyst	M_n [g/mol]	M_w [g/mol]	$Đ$	$[\eta]_w$ [ml/g]	f
Star 1	**7**	13200	15300	1.15	18.0	7.2
Star 2	**8**	8500	13000	1.53	17.5	6.1
Star 3	**1**	12400	25200	2.03	43.7	3.2

The values markedly below those of the linear counterparts for Star 1 and Star 2 prove a branched structure, whereas the difference for Star 3 is significantly less pronounced giving evidence about a lower number of arms. The average number of arms can be estimated by means of the branching ratio g´(M_w), see Equation 1:[38]

$$g'(M_w) = \left(\frac{[\eta]_{branched}}{[\eta]_{linear}}\right)_{M_w} \quad (1)$$

where the subscripts *branched* and *linear* refer to the linear and branched polymer of the same M_w.

From the branching ratio it is possible to calculate the number of arms *f* using the Equation 2:[39]

$$g' = \left[\left(\frac{3f-2}{f^2}\right)^{0.58}\right]\left[\frac{0.724-0.015(f-1)}{0.724}\right] \quad (2)$$

The values of *f* are also listed in Table 5. The Mark-Houwink relation of the linear PLA needed for the calculation of g´(M_w) was obtained by means of six linear PLAs depicted in Figure 5:

$$[\eta] = 0.0158 \times M^{0.803}\ (\text{THF, 25 °C}) \quad (3)$$

These data clearly show a very good agreement between the experimental and the theoretical number of arms for the polymerization tests involving **7** (f = 7.2) and **8** (f = 6.1). On the other hand, the star-shaped PLA prepared using **1** contains a lower number of arms (f = 3.2).

The experimental study unambiguously showed the activation of L-LA through an interaction with the electrophilic tin(II) center in cationic complexes **1**, **4** – **8**, which make them good catalysts in the ROP of L-LA.

Next, the computational study was focused on the first step of the ROP catalytic cycle, which concerns the activation of the L-lactide monomer (Figure 8, Table 6). The coordination of L-LA is exergonic for all cationic complexes with a ΔG ranging from –2.7 to –9.1 kcal mol^{-1}. In line with the topographic steric maps, the structure of the adducts between L-LA and the complexes with a tri-coordinate tin atom (**1**, **4/5** and **6**) is very similar with a notable influence of the bulky ligand L[1] in **4/5**, directing L-LA to a north-western quadrant instead of the south-western in **1** and **6**. In case of **7**, L-LA coordinates cis to the Cl ligand, while it simply replaces the coordinated H_2O molecule in **8**.

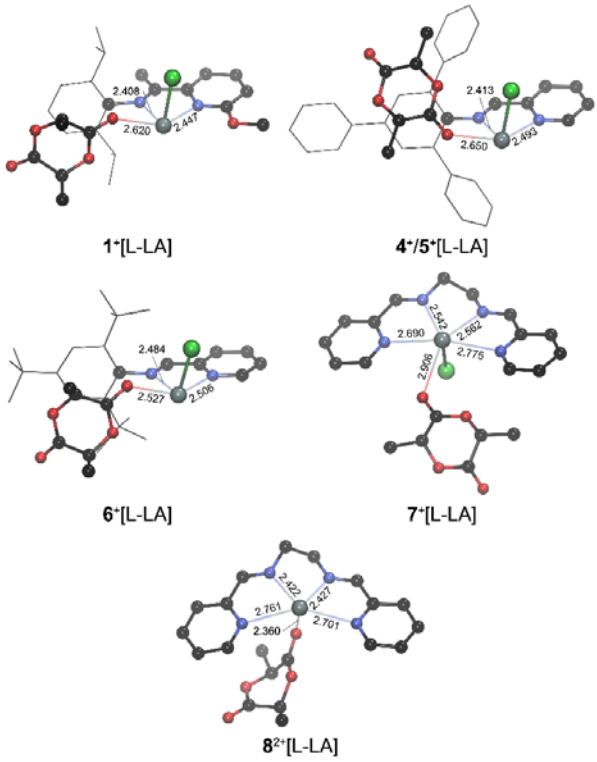

Fig. 8 Optimized geometries of the L-LA adducts $[LSnCl]^+[L\text{-}LA]$ along with selected bond distances (in Å). Hydrogen atoms are omitted for clarity.

Table 6 Gibbs free energy differences (ΔG; in kcal mol^{-1}) for the formation of the L-LA adducts $[LSnCl]^+[L\text{-}LA]$.

	ΔG(DZ)[a]	**ΔG(TZ)**[b]
1$^+$ + [L-LA]→ [**1**]$^+$[L-LA][c]	–9.4	**–5.0**
4$^+$/**5**$^+$ + [L-LA]→ [**4/5**]$^+$[L-LA]	–10.8	**–5.4**
6$^+$ + [L-LA]→ [**6**]$^+$[L-LA]	–14.2	**–8.2**
7$^+$ + [L-LA]→ [**7**]$^+$[L-LA]	–6.8	**–2.7**
8^{2+} + [L-LA]→ [**8**]$^{2+}$[L-LA] + H_2O	–8.1	**–9.1**

[a]Calculated at the B3LYP-D3BJ/cc-pVDZ-PP level of theory; [b]calculated at the B3LYP-D3BJ/cc-pVTZ-PP level of theory.

Table 7 Selected bond lengths (*d*; in Å), Wiberg bond indices (WBI), and NPA atomic charges (*q*; in *e*) for the L-LA adducts [LSnCl]$^+$[L-LA].

	$d_{Sn\text{-}N(Im)}$	$WBI_{Sn\text{-}N(Im)}$	$d_{Sn\text{-}N(Py)}$	$WBI_{Sn\text{-}N(Py)}$	$d_{Sn\text{-}O(LA)}$	$WBI_{Sn\text{-}O(LA)}$	q_{Sn}
[**1**]$^+$[L-LA]	2.408	0.239	2.447	0.196	2.620	0.120	1.26
[**4**/**5**]$^+$[L-LA]	2.413	0.221	2.493	0.174	2.650	0.112	1.32
[**6**]$^+$[L-LA]	2.484	0.226	2.506	0.180	2.527	0.141	1.26
[**7**]$^+$[L-LA]	2.542 2.562	0.175 0.169	2.690 2.775	0.131 0.114	2.906	0.069	1.29
[**8**]$^{2+}$[L-LA]	2.422 2.427	0.230 0.238	2.701 2.761	0.141 0.132	2.360	0.196	1.42

The bond length of the newly formed O→Sn interaction varies in a range of 2.360 – 2.906 Å with a corresponding $WBI_{O\text{-}Sn}$ values between 0.196 and 0.069 (Table 7). Consequently, this leads to a slight elongation of the N→Sn bonds and a negligible change of the NPA charge on the central tin atom.

To further evaluate the plausible effect of the Lewis acidity on the ROP catalytic activity, a Gutmann-Beckett test[40] was performed to quantify the electrophilic nature of the Sn(II) cationic centres in **1**, **6** – **8**, representing the individual types of the prepared cations. The difference in the chemical shift ($\Delta\delta$ in ^{31}P NMR) after the reaction with Ph_3P=O increases in order **7** ($\Delta\delta$ = 0.2 ppm) < **1** ($\Delta\delta$ = 4.0 ppm) < **6** ($\Delta\delta$ = 6.4 ppm) < **8** ($\Delta\delta$ = 11.7 ppm) (see Figure S29, ESI). Thus, the weakest interaction with Ph_3P=O is observed for **7**, while **8** shows the strongest Lewis acidity. These experimental findings were corroborated by the computed fluoride ion affinity (FIA). Accordingly, the lowest FIA value of 547 kJ mol^{-1} was found for **7**, while a value of 955 kJ mol^{-1} was found for **8** (see Table S8, ESI). Furthermore, the order of Lewis acidity correlates very well with the ΔG values of the L-LA activation.

Finally, the activated monomer mechanism, which is initiated by the coordination of the monomer to the catalyst, was confirmed by the reaction of complexes **6** - **8** with L-LA in an equimolar ratio (1:1) at room temperature. ^{1}H and ^{119}Sn NMR monitoring of the mixture of **7** with L-LA did not show any changes in the chemical shifts in comparison with the starting complex **7**. However, the ^{1}H NMR spectra of a more electrophilic **6** (**8**) with L-LA revealed signals with new chemical shifts (see Figure S30 and Figure S32, ESI). Moreover, the ^{119}Sn NMR spectrum of **6** with L-LA showed a signal at δ = –221.2 ppm (see Figure S31, ESI), which is only slightly shifted in comparison to **6** (δ = –224.4 ppm), indicating a weak O→Sn interaction. On the other hand, a signal at δ = –736.0 ppm, corresponding to an upfield shift of 77.6 ppm relative to **8** (δ = –658.0 ppm), was found in the ^{119}Sn NMR spectrum of **8** (see Figure S33, ESI). This clearly demonstrates the strong O→Sn interaction and the formation of an activated monomer **8**[L-LA].

Conclusion

Following the Lewis base mediated ionization of $SnCl_2$ by the α-ketiminopyridine ligand 2-((CH$_3$)C=N(C$_6$H$_3$-2,6-iPr$_2$))-6-CH$_3$O-C$_5$H$_3$N, we reported here the synthesis of a series of tin(II) cations containing the α-iminopyridine ligands $L^{1\text{-}3}$ (L^1 = 2-(CH=N(C$_6$H$_2$-2,4,6-Ph$_3$))C$_5$H$_4$N, L^2 = 2-(CH=N(C$_6$H$_2$-2,4,6-tBu$_3$))C$_5$H$_4$N and L^3 = 1,2-(C$_5$H$_4$N-2-CH=N)$_2$CH$_2$CH$_2$). L^1 and L^2 were shown to be able to stabilize the neutral compounds [$L^{1,2}$→$SnCl_2$], distinguishing them from other N-donor ligands. The preparation of the desired ionic complexes was thus studied in subsequent reactions with an equivalent of $SnCl_2$ or $GaCl_3$ yielding [L^1→SnCl][$SnCl_3$] and [$L^{1,2}$→SnCl][$GaCl_4$]. In contrast, L^3 containing four donor nitrogen atoms showed the ability to autoionize $SnCl_2$ and $Sn(OTf)_2$ affording [L^3→SnCl][$SnCl_3$] and [L^3→Sn(H$_2$O)][OTf]$_2$·THF. The formation of the neutral and ionic complexes was studied by theoretical calculations showing a very good agreement with the experimental work.

The synthesized ionic complexes, together with an earlier reported [{2-((CH$_3$)C=N(C$_6$H$_3$-2,6-iPr$_2$))-6-CH$_3$O-C$_5$H$_3$N}SnCl][$SnCl_3$], were tested as catalysts for the ROP of the L-lactide via an activated monomer mechanism. The kinetic studies indicate a pseudo-first order reaction, and thus a good control over the polymerization. All studied complexes produced linear PLAs with a relatively narrow dispersity *Đ* (1.23-1.45). The computational study was also focused on the activation of the L-lactide monomer. The coordination of L-LA is exergonic for all cationic complexes supporting the formation of the activated monomer and the proposed mechanism. The experimental and computational studies unambiguously showed the activation of L-LA through an interaction with the electrophilic tin(II) center in cationic complexes **1**, **4** – **8**, which makes them good catalysts in the ROP of L-LA.

Moreover, complexes [L^3→SnCl][$SnCl_3$] and [L^3→Sn(H$_2$O)][OTf]$_2$·THF proved to be the versatile catalysts as they produced not only the linear but also the star-shaped PLA with a dipentaerythritol core. The experimental number of arms fitted very well with the theoretical ones. This fact will be further studied with other cyclic ester monomers as well as with other polyalcohols as core.

Experimental part

General Consideration

All moisture and air sensitive reactions were carried out under an argon atmosphere using standard Schlenk tube techniques. All solvents were dried using Pure Solv–Innovative Technology equipment. Starting compounds L^{1-3} and **1** were prepared according to the literature.[41-43] $SnCl_2$, $GaCl_3$ and $Sn(OTf)_2$ were purchased from Sigma Aldrich and used as received. L-lactide was purchased from Sigma-Aldrich and recrystallized from toluene before use. Elemental analyses were performed on an LECO-CHNS-932 analyser. The ^1H, ^{13}C and ^{119}Sn NMR spectra were recorded on a Bruker 500 NMR spectrometer at 298 K. The ^1H and ^{13}C NMR spectra were referenced internally to the residual protio-solvent. The ^{119}Sn NMR spectra were referenced externally to Me_4Sn. Mass spectra were measured using a LTQ Orbitrap XL MALDI mass spectrometer (Thermo Fisher Scientific, Waltham, MA, USA) with a nitrogen UV laser with a beam size of 80-100 µm. SEC-MALS-Visco measurements were carried out using an experimental set-up consisting of an Agilent Infinity II 1260 liquid chromatograph coupled with a MALS detector DAWN, an online viscometer ViscoStar and a refractive index (RI) detector Optilab (all detectors from Wyatt Technology). The separation was performed by means of two PLgel Mixed-C 300 × 7.5 mm columns from Agilent. Tetrahydrofuran (THF) was used as the mobile phase at a flow rate of 1 mL/min. The samples were prepared in THF at the concentration of 5 mg/mL, filtered with 0.45 µm filter and injected in the volume of 100 µL.

Syntheses

Synthesis of [{2-(CH=N(C_6H_2-2,4,6-Ph_3))C_5H_4N}$SnCl_2$] (2). A solution of $SnCl_2$ (50 mg, 0.26 mmol) in THF (10 mL) was added to a stirred solution of ligand L^1 (0.11 g, 0.26 mmol) in THF (10 mL). The reaction mixture was stirred for 24 h at room temperature. After that all volatiles were removed under reduced pressure. The residue was washed with toluene-hexane (1:1) giving compound **2** as an orange powder material. Yield: 0.15 g (94 %). For **2**: mp = 150.6-152.0 °C. Anal.Calcd.for $C_{30}H_{22}Cl_2N_2Sn$ (MW 600.09): C, 60.0; H, 3.7. Found: C, 60.2; H, 3.8. ^1H NMR (THF-d_8, 500.13 MHz, 25 °C): δ *(ppm)* 7.15-7.18 (m, 2H, Ar-H), 7.23-7.27 (m, 6H, Ar-H), 7.37-7.41 (m, 3H, Ar-H), 7.47 (d, 4H, Ar-H, $^3J(^1H,^1H)$ = 7.3 Hz), 7.66 (s, 2H, Ar-H), 7.70 (d, 2H, Ar-H, $^3J(^1H,^1H)$ = 7.5 Hz), 7.75-7.80 (m, 2H, Ar-H), 8.11 (s, 1H, CH=N), 8.84 (d, 1H, Ar-H, $^3J(^1H,^1H)$ = 5.0 Hz). ^{13}C NMR (THF-d_8, 125.72 MHz, 25 °C): δ *(ppm)* 124.2, 126.9, 127.8, 128.3, 129.0, 129.6, 129.8, 130.3, 131.3, 135.4, 138.8, 139.4, 140.9, 141.4, 147.2, 150.6, 154.0 (Ar-C), 166.2 (CH=N). ^{119}Sn NMR (THF-d_8, 186.36 MHz, 25 °C) δ *(ppm)* –227.1.

Synthesis of [{2-(CH=N(C_6H_2-2,4,6-tBu_3))C_5H_4N}$SnCl_2$] (3). A solution of $SnCl_2$ (55 mg, 0.29 mmol) in THF (10 mL) was added to a stirred solution of ligand L^2 (0.10 g, 0.29 mmol) in THF (10 mL). The reaction mixture was stirred for 24 h at room temperature. After that all volatiles were removed under reduced pressure. The residue was washed with toluene-hexane (1:1) giving compound **3** as an orange powder material. Yield: 0.14 g (90 %). For **3**: mp = 148.3-149.5 °C. Anal.Calcd.for $C_{24}H_{34}Cl_2N_2Sn$ (MW 540.15): C, 53.4; H, 6.3. Found: C, 53.2; H, 6.2. ^1H NMR (THF-d_8, 500.13 MHz, 25 °C): δ *(ppm)* 1.25 (s, 18H, tBu), 1.28 (s, 9H, tBu), 7.31 (s, 2H, Ar-H), 7.40 (m, 1H, Ar-H), 7.87 (m, 1H, Ar-H), 8.17 (s, 1H, CH=N), 8.20 (d, 1H, Ar-H, $^3J(^1H,^1H)$ = 7.6 Hz), 8.65 (d, 1H, Ar-H, $^3J(^1H,^1H)$ = 4.6 Hz). ^{13}C NMR (THF-d_8, 125.72 MHz, 25 °C): δ *(ppm)* 32.1 (C(CH$_3$)$_3$), 32.2 ((C(CH$_3$)$_3$), 35.4 (C(CH$_3$)$_3$), 36.6 (C(CH$_3$)$_3$), 122.2, 122.5, 126.5, 138.0, 138.9, 145.3, 150.8, 150.9, 155.1 (Ar-C), 164.8 (CH=N). ^{119}Sn NMR (THF-d_8, 186.36 MHz, 25 °C) δ *(ppm)* –219.4.

Synthesis of [{2-(CH=N(C_6H_2-2,4,6-Ph_3))C_5H_4N}SnCl][$SnCl_3$] (4). A solution of $SnCl_2$ (32 mg, 0.17 mmol) in THF (10 mL) was added to a stirred solution of **2** (0.10 g, 0.17 mmol) in THF (10 mL). The reaction mixture was stirred for 24 h at room temperature. After that all volatiles were removed under reduced pressure. The residue was washed with toluene-hexane (1:1) giving compound **4** as a yellow powder material. Yield: 0.12 g (90 %). For **4**: mp = 195.7-198.3 °C (with decomp.). Anal.Calcd.for $C_{30}H_{22}Cl_4N_2Sn_2$ (MW 789.74): C, 45.6; H, 2.8. Found: C, 45.3; H, 2.7. ^1H NMR (THF-d_8, 500.13 MHz, 25 °C): δ *(ppm)* 7.20 (m, 2H, Ar-H), 7.25-7.70 (m, 5H, Ar-H), 7.39 (m, 2H, Ar-H), 7.52 (d, 4H, Ar-H, $^3J(^1H,^1H)$ = 7.3 Hz), 7.58 (t, 1H, Ar-H, $^3J(^1H,^1H)$ = 6.4 Hz), 7.67-7.71 (m, 5H, Ar-H), 7.98 (t, 1H, Ar-H, $^3J(^1H,^1H)$ = 7.6 Hz), 8.33 (s, 1H, CH=N), 9.30 (d, 1H, Ar-H, $^3J(^1H,^1H)$ = 4.3 Hz). ^{13}C NMR (THF-d_8, 125.72 MHz, 25 °C): δ *(ppm)* 122.8, 124.0, 124.5, 124.9, 125.0, 125.4, 126.2, 126.5, 126.6, 126.7, 126.8, 127.3, 128.4, 132.7, 136.7, 137.8, 138.2, 138.4, 139.0, 139.2, 143.4 (Ar-C), 147.7 (CH=N), 150.1, 163.0 (Ar-C). ^{119}Sn NMR (THF-d_8, 186.36 MHz, 25 °C) δ *(ppm)* -235.4. ^{119}Sn NMR (THF-d_8, 186.36 MHz, -50 °C) δ *(ppm)* –254.9, –347.6. MALDI – Orbitrap MS: m/z = 565.04 [{2-(CH=N(C_6H_2-2,4,6-Ph_3))C_5H_4N}SnCl]$^+$ (66 %), m/z = 226.80 [$SnCl_3$]$^-$ (92 %).

Synthesis of [{2-(CH=N(C_6H_2-2,4,6-Ph_3))C_5H_4N}SnCl][$GaCl_4$] (5). A solution of $GaCl_3$ (14 mg, 0.08 mmol) in THF (10 mL) was added to a stirred solution of **2** (48 mg, 0.08 mmol) in THF (10 mL). The reaction mixture was stirred for 24 h at room temperature. After that all volatiles were removed under reduced pressure. The residue was washed with toluene-hexane (1:1) giving compound **5** as a yellow powder material. Yield: 55 mg (89 %). For **5**: mp = 187.3-189.6 °C (with decomp.). Anal.Calcd.for $C_{30}H_{22}Cl_5N_2SnGa$ (MW 776.19): C, 46.4; H, 2.9. Found: C, 46.3; H, 2.8. ^1H NMR (THF-d_8, 500.13 MHz, 25 °C): δ *(ppm)* 7.25 (m, 2H, Ar-H), 7.35 (m, 5H, Ar-H), 7.49 (m, 3H, Ar-H), 7.50 (m, 5H, Ar-H), 7.74 (m, 2H, Ar-H), 7.96 (s, 2H, Ar-H), 8.44 (m, 1H, Ar-H), 8.47 (s, 1H, CH=N), 8.84 (d, 1H, Ar-H, $^3J(^1H,^1H)$ = 6.2 Hz). ^{13}C NMR (THF-d_8, 125.72 MHz, 25 °C): δ *(ppm)* 126.2, 126.5, 126.9, 127.5, 127.6, 127.8, 128.4, 128.5, 128.6, 128.8, 128.9, 128.9, 129.2, 129.5, 130.3, 135.0, 138.9, 139.3, 139.5, 140.0, 140.4 (Ar-C), 143.2 (CH=N), 145.8, 161.3 (Ar-C). ^{119}Sn NMR (THF-d_8, 186.36 MHz, 25 °C) δ *(ppm)* –235.5. MALDI – Orbitrap MS: m/z = 565.05 [{2-(CH=N(C_6H_2-2,4,6-Ph_3))C_5H_4N}SnCl]$^+$ (34 %), m/z = 210.79 [$GaCl_4$]$^-$ (100 %).

Synthesis of [{2-(CH=N(C_6H_2-2,4,6-tBu_3))C_5H_4N}SnCl][$GaCl_4$] (6). A solution of $GaCl_3$ (11 mg, 0.06 mmol) in THF (10 mL) was

added to a stirred solution of **3** (32 mg, 0.06 mmol) in THF (10 mL). The reaction mixture was stirred for 24 h at room temperature. After that all volatiles were removed under reduced pressure. The residue was washed with toluene-hexane (1:1) giving compound **6** as a yellow powder material. Yield: 38 mg (88 %). For **6**: mp = 183.1-185.5 °C (with decomp.). Anal.Calcd.for $C_{24}H_{34}Cl_5N_2SnGa$ (MW 716.23): C, 40.3; H, 4.8. Found: C, 40.5; H, 4.9. ^{1}H NMR (THF-d_8, 500.13 MHz, 25 °C): δ *(ppm)* 1.27 (s, 18H, tBu), 1.30 (s, 9H, tBu), 7.37 (s, 2H, Ar-H), 8.13 (m, 1H, Ar-H), 8.41 (d, 1H, Ar-H), 8.44 (s, 1H, CH=N), 8.66 (m, 1H, Ar-H), 8.98 (d, 1H, Ar-H). ^{13}C NMR (THF-d_8, 125.72 MHz, 25 °C): δ *(ppm)* 32.0 (C(CH_3)$_3$), 32.4 ((C(CH_3)$_3$), 35.6 (*C*(CH_3)$_3$), 36.7 (*C*(CH_3)$_3$), 122.7, 122.9, 128.4, 129.9, 139.2, 146.8, 147.2, 149.4 (Ar-C) (1 signal not found), 159.4 (CH=N). ^{119}Sn NMR (THF-d_8, 186.36 MHz, 25 °C) δ *(ppm)* –224.4. MALDI – Orbitrap MS: m/z = 505.14 [{2-(CH=N(C_6H_2-2,4,6-*t*Bu_3))C_5H_4N}SnCl]$^+$ (2 %), m/z = 210.79 $[GaCl_4]^-$ (100 %).

Synthesis of [{1,2-(C_5H_4N-2-CH=N)$_2CH_2CH_2$}SnCl][$SnCl_3$] (7). A solution of $SnCl_2$ (0.40 g, 2.10 mmol) in THF (20 mL) was added to a stirred solution of L[3] (0.25 g, 1.05 mmol) in THF (20 mL). The reaction mixture was stirred for 24 h at room temperature. After that all volatiles were removed under reduced pressure. The residue was washed with toluene-hexane (1:1) giving compound **7** as an orange powder material. Yield: 0.56 g (86 %). For **7**: mp = 186.9-188.5 °C (with decomp.). Anal.Calcd.for $C_{14}H_{14}Cl_4N_2Sn_2$ (MW 617.52): C, 27.2; H, 2.3. Found: C, 27.0; H, 2.1. ^{1}H NMR (CD_3CN, 500.13 MHz, 25 °C): δ *(ppm)* 4.23 (s, 4H, CH_2), 7.76 (m, 2H, Ar-H), 8.00 (dt, 2H, Ar-H, ^3J(^{1}H,^{1}H) = 7.6 Hz), 8.17 (td, 2H, Ar-H, ^3J(^{1}H,^{1}H) = 7.6 Hz), 8.92 (d, 2H, Ar-H, ^3J(^{1}H,^{1}H) = 4.9 Hz), 9.02 (s, 2H, CH=N). ^{13}C NMR (CD_3CN, 125.72 MHz, 25 °C): δ *(ppm)* 56.9 (CH_2), 129.7, 130.1, 141.1, 149.3, 149.9 (Ar-C), 166.7 (CH=N). ^{119}Sn NMR (CD_3CN, 186.36 MHz, 25 °C) δ *(ppm)* –25.5, –592.6.

Synthesis of [{1,2-(C_5H_4N-2-CH=N)$_2CH_2CH_2$}Sn(H_2O)][OTf]$_2$·THF (8). A solution of Sn(OTf)$_2$ (0.52 g, 1.26 mmol) in THF (20 mL) was added to a stirred solution of L[3] (0.30 g, 1.26 mmol) in THF (20 mL). The reaction mixture was stirred for 24 h at room temperature. During this time a yellow solid was precipitated and then collected by filtration. The solid was washed with hexane giving compound **8** as a yellow powder material. Yield: 0.70 g (75 %). For **8**: mp = 200.1-203.8 °C (with decomp.). Anal.Calcd.for $C_{20}H_{24}O_8F_6N_4S_2Sn$ (MW 745.26): C, 32.2; H, 3.3. Found: C, 32.0; H, 3.2. ^{1}H NMR (CD_3CN, 500.13 MHz, 25 °C): δ *(ppm)* 1.79 (m, 4H, CH_2-THF), 3.63 (m, 4H, CH_2-THF), 4.26 (s, 4H, CH_2), 7.79 (t, 2H, Ar-H, ^3J(^{1}H,^{1}H) = 5.6 Hz), 8.00 (d, 2H, Ar-H, ^3J(^{1}H,^{1}H) = 7.6 Hz), 8.17-8.21 (m, 2H, Ar-H), 8.93 (bs, 2H, Ar-H), 9.08 (s, 2H, CH=N). ^{13}C NMR (CD_3CN, 125.72 MHz, 25 °C): δ *(ppm)* 26.5 (CH_2-THF), 56.7 (CH_2), 68.6 (CH_2-THF), 121.7 (q, CF_3, ^1J(^{19}F, ^{13}C = 320 Hz), 130.0, 130.1, 141.7, 149.2, 150.4 (Ar-C), 167.9 (CH=N). ^{19}F NMR (CD_3CN, 470.59 MHz, 25 °C) δ *(ppm)* -79.4. ^{119}Sn NMR (CD_3CN, 186.36 MHz, 25 °C) δ *(ppm)* –658.0.

Ring-Opening Polymerization of L-lactide Using 3-8 as Catalysts. *Typical polymerization procedures are as follows.* A monomer, catalyst and alcohol in a molar ratio 100:1:1 were weighted into a Schlenk tube and homogenized. The polymerization mixture was then placed into an oven preheated to 145 °C. After a desired time, the reaction mixture was cooled to room temperature and subjected to the ^{1}H NMR analysis. The monomer conversion was determined by the calculation of the integration of the monomer vs polymer methyl or methine resonance in the ^{1}H NMR ($CDCl_3$, 500 MHz) spectrum. The polymer was purified by dissolving the crude samples in CH_3Cl and precipitating into cold methanol (100 mL). The obtained polymers were dried to a constant weight, and the dry polymer samples were analyzed by the SEC.

Crystallography

The X-ray data for colorless crystals of **2**, (see Tables S1) were obtained at 150K using Oxford Cryostream low-temperature device on a Nonius KappaCCD diffractometer with Mo K_α radiation (λ = 0.71073 Å), a graphite monochromator, and the ϕ and χ scan mode. Data reductions were performed with DENZO-SMN[44]. The absorption was corrected by multi-scan method – SADABS or by integration methods.[45] Structures were solved by direct methods (Sir92)[46] and refined by full matrix least-square based on F^2 (SHELXL97)[47].

Full-set of diffraction data for **7** and **8** (see Tables S2, S3) were collected at 150(2)K with a Bruker D8-Venture diffractometer equipped with Cu (Cu/Kα radiation; λ = 1.54178 Å) or Mo (Mo/Kα radiation; λ = 0.71073 Å) microfocus X-ray (IμS) sources, Photon CMOS detector and Oxford Cryosystems cooling device was used for data collection.

The frames were integrated with the Bruker SAINT software package using a narrowframe algorithm. Data were corrected for absorption effects using the Multi-Scan method (SADABS). Obtained data were treated by XT-version 2014/5 and SHELXL-2017/1 software implemented in APEX3 v2016.5-0 (Bruker AXS) system.[48]

Hydrogen atoms were mostly localized on a difference Fourier map, however to ensure uniformity of treatment of crystal, all hydrogen were recalculated into idealized positions (riding model) and assigned temperature factors H_{iso}(H) = 1.2 U_{eq} (pivot atom) or of 1.5U_{eq} (methyl). H atoms in methyl, methylene, moieties and hydrogen atoms in aromatic rings were placed with C-H distances of 0.96, 0.97, and 0.93Å. Hydrogen atoms of O-H groups were refined freely or with fixed distances of 0.82Å. Disordered parts of OTf group and coordinated THF molecules in **8** were treated by standard methods.

Crystallographic data for structural analysis have been deposited with the Cambridge Crystallographic Data Centre, CCDC nos. 2078257-2078259 for **2**, **7** and **8**. Copies of this information may be obtained free of charge from The Director, CCDC, 12 Union Road, Cambridge CB2 1EY, UK (fax: +44-1223-336033; e-mail: deposit@ccdc.cam.ac.uk or www: http://www.ccdc.cam.ac.uk).

Computational details

All calculations were carried out by using DFT as implemented in the Gaussian 16 quantum chemistry program.[49] Geometry optimizations were performed at the B3LYP-

D3BJ[30]/cc-pVDZ[31a,b] level of theory including Grimme DFT-D3 empirical dispersion with the Becke Johnson damping function (cc-pVDZ-PP[31c,d] basis set, including small-core energy-consistent relativistic pseudopotentials that account also for relativistic effects, was used for Sn). The electronic energies of the optimized structures were re-evaluated by additional single-point calculations on each of the optimized geometries by using the triple-ζ quality cc-pVTZ(-PP) basis set.[31] Analytical vibrational frequencies within the harmonic approximation were computed with the cc-pVDZ(-PP) basis set to confirm a proper convergence to well-defined minima or saddle points on the potential energy surface. The Gibbs free energies G^{solv}(cc-pVTZ) used to calculate the energy differences reported in this article were computed by using Equations (4)-(7),

$$G^{solv}(\text{cc-pVTZ}) = G(\text{cc-pVTZ}) + \text{SC} \quad (4)$$

$$G(\text{cc-pVTZ}) = E(\text{cc-pVTZ}) + \text{TC} \quad (5)$$

$$\text{TC} = G(\text{cc-pVDZ}) - E(\text{cc-pVDZ}) \quad (6)$$

$$\text{SC} = E^{solv}(\text{cc-pVDZ}) - E(\text{cc-pVDZ}) \quad (7)$$

in which E(x) is the self-consistent field electronic energy derived from the cc-pVDZ or cc-pVTZ basis sets, TC is the thermal correction to the energy calculated with the cc-pVDZ basis set, G(cc-pVDZ) is the free energy at 298.15 K for the double-ζ quality basis set, SC is the solvent correction for E^{solv}(cc-pVDZ), which is the self-consistent field energy in the implicit Solvation Model based on Density (SMD)[50] using THF (ε = 7.4257) as solvent, calculated with the cc-pVDZ basis set.

The natural bond orbital (NBO) analysis[33] and calculations of the Wiberg bond indices[32] were performed using NBO 3.0 program as implemented in the Gaussian 16[49] package at the B3LYP-D3BJ/cc-pVTZ(-PP) level of theory.

SambVca 2.1 web application was used to calculate the percentage buried volume (%V_{Bur})[35] and topographic steric maps of ligands.[34] %V_{Bur} quantifies the fraction of the first coordination sphere around a metal center occupied by the ligand, while the topographic steric maps allow for 3D visualization of the shape of the catalytic pocket.

The Ziegler-Rauk energy decomposition analysis[36] was carried out on the optimized structures at the ZORA[51]/B3LYP-D3BJ[30]/TZ2P[52] level of theory using Amsterdam Modeling Suite (AMS2020; ADF engine).[53] The interaction energy ΔE_{int} between two fragments can be decomposed into physically meaningful terms within Kohn–Sham MO theory [Equation (8)],

$$\Delta E_{int} = \Delta E_{Pauli} + \Delta V_{elst} + \Delta E_{oi} + E_{disp} \quad (8)$$

where E_{disp} is the dispersion energy and ΔE_{Pauli}, ΔV_{elst}, and ΔE_{oi} are the Pauli repulsion, electrostatic interaction, and orbital interaction between fragments, respectively. The dispersion energy accounts for the van der Waals interaction between fragments. The Pauli repulsion is the result of the steric repulsion between fragments, caused by the destabilizing interaction between electrons with identical spin. ΔV_{elst} represents the quasi-classical electrostatic interaction between the unperturbed charge distributions of the two fragments. The ΔE_{oi} term originates from orbital interactions, charge transfer, and polarization.

Fluoride ion affinities (FIA) were calculated at the PW6B95-D3BJ[54]/def2-QZVPP[55] level of theory according to the procedure suggested by Greb using the TMS-system as an anchor point for the FIA computations via (pseudo-)isodesmic reactions.[56]

Conflicts of interest

There are no conflicts to declare.

Acknowledgements

The authors would like to thank the Czech Science Foundation (no. 20-10417S). JT gratefully acknowledges the financial support of the Research Foundation–Flanders (FWO; Project No. 12Y7721N) and the computational resources and services provided by the VUB-HPC (VSC Tier-2 cluster of the Flemish Supercomputer Center) funded by the Vrije Universiteit Brussel, FWO and the Flemish Government.

Notes and references

1 (a) A.-Ch. Albertsson, I. K. Varma, In: *Degradable Aliphatic Polyesters. Advances in Polymer Science*, 2002, **157**, Springer, Berlin, Heidelberg. (b) M. Vert, *Biomacromolecules*, 2005, **6**, 538. (c) Ch. K. Williams, *Chem. Soc. Rev.*, 2007, **36**, 1573.

2 A. N. Vaidya, R. A. Pandey, S. Mudliar, M. S. Kumar, T. Chakrabarti, S. Devotta, *Crit. Rev. Environ. Sci. Technol.*, 2005, **35**, 429.

3 (a) Y. Ikada, H. Tsuji, *Macromol. Rapid Commun.*, 2000, **21**, 117. (b) G.-Q. Chen, *Chem. Soc. Rev.*, 2009, **38**, 2434. (c) S. Farah, D. G. Anderson, R. Langer, *Adv. Drug Delivery Rev.*, 2016, **107**, 367.

4 (a) Poly(lactic acid): Synthesis, Structures, Properties, Processing and Applications; R. Auras, L.-T. Lim, S. E. M. Selke, H. Tsuji, Eds.; John Wiley and Sons Inc.: Hoboken, NJ, 2010.

5 (a) J. C. Wu, T. L. Yu, C. T. Chen, C. C. Lin, *Coord. Chem. Rev.*, 2006, **250**, 602. (b) C. M. Thomas, *Chem. Soc. Rev.*, 2010, **39**, 165. (c) Y. Wei, S. Wang, S. Zhoua, *Dalton Trans.*, 2016, **45**, 4471. (d) J. Gao, D. Zhu, W. Zhang, G. A. Solan, Y. Ma, W.-H. Sun, *Inorg. Chem. Front.*, 2019, **6**, 2619. (e) Y. Sarazin, J.-F. Carpentier, *Chem. Rev.*, 2015, **115**, 3564. (f) A. Hermann, S. Hill, A. Metz, J. Heck, A. Hofmann, L. Hartmann, S. Herres-Pawlis, *Angew. Chem. Int. Ed.*, 2020, **59**, 21778. (g) P. M. Schäfer, P. McKeown, M. Fuchs, R. D. Rittinghaus, A. Hermann, J. Henkel, S. Seidel, Ch. Roitzheim, A. N. Ksiazkiewicz, A. Hofmann, A. Pich, M. D. Jones, S. Herres-Pawlis, *Dalton Trans.*, 2019, **48**, 6071. (h) P. M. Schäfer, S. Herres-Pawlis, *ChemPlusChem*, 2020, **85**, 1044.

6 In Handbook of Ring-Opening Polymerization; P. Dubois, O. Coulembier, J.-M. Raquez,.; Eds.; Wiley-VCH: Weinheim, 2009.

7 V.S.V.S.N. Swamy, S. Pal, S. Khan, S. S. Sen, *Dalton Trans.*, 2015, **44**, 12903.

8 P. Jutzi, F. Kohl, P. Hofmann, C. Krüger, Y.-H. Tsay, *Chem. Ber.*, 1980, **113**, 757.

9 H. V. R Dias, W. Jin, *J. Am. Chem. Soc.*, 1996, **118**, 9123.

10 M. J. Taylor, A. J. Saunders, M. P. Coles, J. R. Fulton, *Organometallics*, 2011, **30**, 1334.

11 J. Li, Ch. Schenk, F. Winter, H. Scherer, N. Trapp, A. Higelin, S. Keller, R. Pöttgen, I. Krossing, C. Jones, *Angew. Chem. Int. Ed.*, 2012, **51**, 9557.

12 V. Poirier, T. Roisnel, S. Sinbandhit, M. Bochmann, J.-F. Carpentier, Y. Sarazin, *Chem. Eur. J.*, 2012, **18**, 2998.
13 S. Khan, G. Gopakumar, W. Thiel, M. Alcarazo, *Angew. Chem. Int. Ed.*, 2013, **52**, 5644.
14 P. A. Gray, K. D. Krause, N. Burford, B. O. Patrick, *Dalton Trans.*, 2017, **46**, 8363.
15 A. P. Singh, H. W. Roesky, E. Carl, D. Stalke, J.-P. Demers, A. Lange, *J. Am. Chem. Soc.*, 2012, **134**, 4998.
16 M. Bouška, L. Dostál, A. Růžička, R. Jambor, *Organometallics*, 2013, **32**, 1995.
17 (a) T. Jurca, L. K. Hiscock, I. Korobkov, Ch. N. Rowley, D. S. Richeson, *Dalton Trans.*, 2014, **43**, 690. (b) E. Magdzinski, P. Gobbo, M. S. Workentin, P. J. Ragogna, *Inorg. Chem.*, 2013, **52**, 11311.
18 R. K. Raut, M. Majumdar, *J. Organomet. Chem.*, 2019, **887**, 18.
19 F. S. Tschernuth, F. Hanusch, T. Szilvási, S. Inoue, *Organometallics*, 2020, **39**, 4265.
20 J. C. Avery, M. A. Hanson, R. H. Herber, K. J. Bladek, P. A. Rupar, I. Nowik, Y. Huang, K. M. Baines, *Inorg. Chem.*, 2012, **51**, 7306.
21 Ch. L. B. Macdonald, R. Bandyopadhyay, B. F. T. Cooper, W. W. Friedl, A. J. Rossini, R. W. Schurko, S. H. Eichhorn, R. H. Herber, *J. Am. Chem. Soc.*, 2012, **134**, 4332.
22 M. Gawron, Ch. Dietz, M. Lutter, A. Duthie, V. Jouikov, K. Jurkschat, *Chem. Eur. J.*, 2015, **21**, 16609.
23 A. Schäfer, F. Winter, W. Saak, D. Haase, R. Pöttgen, T. Müller, *Chem. Eur. J.*, 2011, **17**, 10979.
24 R. K. Raut, P. Sahoo, D. Chimnapure, M. Majumdar, *Dalton Trans.*, 2019, **48**, 10953.
25 M. Ibarra-Rodríguez, B. M. Muñoz-Flores, H. V. R Dias, I. F. Hernández-Ahuactzi, M. Sánchez, V. M. Jiménez-Pérez, *Arab. J. Chem.*, 2019, **12**, 5120.
26 S. V. Vasnin, J. Cetrullo, R. A. Geanangel, I. Bernal, *Inorg. Chem.*, 1990, **29**, 885.
27 S. J. Archer, K. R. Koch, S. Schmidt, *Inorganica Chim. Acta*, 1987, **23**, 209.
28 M. Mantina, A. C. Chamberlin, R. Valero, Ch. J. Cramer, D. G. Truhlar, *J. Phys. Chem. A*, 2009, **113**, 5806.
29 (a) M. Henn, V. Deáky, S. Krabbe, M. Schürmann, M. H. Prosenc, S. Herres-Pawlis, B. Mahieu, K. Jurkschat, *Z. Anorg. Allg. Chem.*, 2011, **637**, 211. (b) M. Wagner, Ch. Dietz, M. Bouška, L. Dostál, Z. Padělková, R. Jambor, K. Jurkschat, *Organometallics*, 2013, *32*, 4973.
30 (a) S. H. Vosko, L. Wilk and M. Nusair, *Can. J. Phys.*, 1980, **58**, 1200; (b) C. Lee, W. Yang and R. G. Parr, *Phys. Rev. B*, 1988, **37**, 785; (c) A. D. Becke, *J. Chem. Phys.*, 1993, **98**, 5648; (d) P. J. Stephens, F. J. Devlin, C. F. Chabalowski and M. J. Frisch, *J. Phys. Chem.*, 1994, **98**, 11623; (e) S. Grimme, J. Antony, S. Ehrlich and H. Krieg, *J. Chem. Phys.*, 2010, **132**, 154104.
31 (a) T. H. Dunning, *J. Chem. Phys.*, 1989, **90**, 1007; (b) D. E. Woon and T. H. Dunning, *J. Chem. Phys.*, 1993, **98**, 1358; (c) B. Metz, H. Stoll and M. Dolg, *J. Chem. Phys.*, 2000, **113**, 2563; (d) K. A. Peterson, *J. Chem. Phys.*, 2003, **119**, 11099.
32 K. B. Wiberg, *Tetrahedron*, 1968, **24**, 1083.
33 (a) J. P. Foster and F. Weinhold, *J. Am. Chem. Soc.*, 1980, **102**, 7211; (b) F. Weinhold, *J. Comput. Chem.*, 2012, **33**, 2363, and references therein; (c) C. R. Landis and F. Weinhold, in *The Chemical Bond: Fundamental Aspects of Chemical Bonding*, ed. G. Frenking and S. Shaik, Wiley-VCH, Weinheim, 2014, ch. 3, pp. 91-120.
34 A. Poater, B. Cosenza, A. Correa, S. Giudice, F. Ragone, V. Scarano and L. Cavallo, *Eur. J. Inorg. Chem.*, 2009, 1759.
35 L. Falivene, Z. Cao, A. Petta, L. Serra, A. Poater, R. Oliva, V. Scarano and L. Cavallo, *Nat. Chem.*, 2019, **11**, 872.
36 (a) T. Ziegler and A. Rauk, *Theor. Chim. Acta*, 1977, **46**, 1; (b) T. Ziegler and A. Rauk, *Inorg. Chem.*, 1979, **18**, 1558; (c) T. Ziegler and A. Rauk, *Inorg. Chem.*, 1979, **18**, 1755; (d) F. M. Bickelhaupt and E. J. Baerends, in *Reviews in Computational Chemistry*, ed. K. B. Lipkowitz and D. B. Boyd, Wiley, New York, 2000, vol. 15, ch. 1, pp. 1-86.
37 M. Save, M. Schappacher, A. Soum, *Macromol. Chem. Phys.*, 2002, **203**, 889.
38 S. Podzimek, Light Scattering, Size Exclusion Chromatography and Asymmetric Flow Field Flow Fractionation: Powerful Tools for the Characterization of Polymers, Proteins and Nanoparticles, Wiley **2011**, ISBN: 9780470877975.
39 J. Douglas, J. Roovers, K. Freed, *Macromolecules*, 1990, **23**, 4168.
40 (a) U. Mayer, V. Gutmann, W. Gerger, *Monatsh. Chem.*, 1975, **106**, 1235. (b) V. Gutmann, *Coord. Chem. Rev.*, 1976, **18**, 225. (c) M. A. Beckett, D. S. Brassington, S. J. Coles, M. B. Hursthouse, *Inorg. Chem. Commun.*, 2000, **3**, 530. (d) M. A. Beckett, D. S. Brassington, M. E. Light, M. B. Hursthouse, *J. Chem. Soc., Dalton. Trans.*, 2001, 1768. (e) M. A. Beckett, G. C. Strickland, J. R. Holland, K. S. Varma, *Polym. Commun.*, 1996, 37, 4629.
41 J. Raynaud, J. Y. Wu, T. Ritter, *Angew. Chem. Int. Ed.*, 2012, **51**, 11805.
42 R. E. Murray, *PCT Int. Appl.*, 1999, WO 9901460 A1 19990114.
43 G. Amenuvor, Ch. K. Rono, J. Darkwa, B. C. E. Makhubela, *Eur. J. Inorg. Chem.*, 2019, 3942.
44 Z. Otwinowski, W. Minor, *Methods Enzymol*,, 1997, **276**, 307.
45 P. Coppens, In: F.R. Ahmed, S.R. Hall, C.P. Huber, Editors, Crystallographic Computing, 1970, 255, Copenhagen, Munksgaard.
46 A. Altomare, G. Cascarano, C. Giacovazzo, A. Guagliardi, *J. Appl. Cryst.* 1994, **27**, 1045.
47 G. M. Sheldrick, SHELXL-97, University of Göttingen: Göttingen, **2008**.
48 G. M. Sheldrick, SHELXT. *Acta Cryst.* 2015, **A71**, 3.
49 Gaussian 16, Revision A.03, M. J. Frisch, G. W. Trucks, H. B. Schlegel, G. E. Scuseria, M. A. Robb, J. R. Cheeseman, G. Scalmani, V. Barone, G. A. Petersson, H. Nakatsuji, X. Li, M. Caricato, A. V. Marenich, J. Bloino, B. G. Janesko, R. Gomperts, B. Mennucci, H. P. Hratchian, J. V. Ortiz, A. F. Izmaylov, J. L. Sonnenberg, D. Williams-Young, F. Ding, F. Lipparini, F. Egidi, J. Goings, B. Peng, A. Petrone, T. Henderson, D. Ranasinghe, V. G. Zakrzewski, J. Gao, N. Rega, G. Zheng, W. Liang, M. Hada, M. Ehara, K. Toyota, R. Fukuda, J. Hasegawa, M. Ishida, T. Nakajima, Y. Honda, O. Kitao, H. Nakai, T. Vreven, K. Throssell, J. A. Montgomery, Jr., J. E. Peralta, F. Ogliaro, M. J. Bearpark, J. J. Heyd, E. N. Brothers, K. N. Kudin, V. N. Staroverov, T. A. Keith, R. Kobayashi, J. Normand, K. Raghavachari, A. P. Rendell, J. C. Burant, S. S. Iyengar, J. Tomasi, M. Cossi, J. M. Millam, M. Klene, C. Adamo, R. Cammi, J. W. Ochterski, R. L. Martin, K. Morokuma, O. Farkas, J. B. Foresman, and D. J. Fox, Gaussian, Inc., Wallingford CT, 2016.
50 A. V. Marenich, C. J. Cramer and D. G. Truhlar, *J. Phys. Chem. B*, 2009, **113**, 6378.
51 (a) E. van Lenthe, E. J. Baerends and J. G. Snijders, *J. Chem. Phys.*, 1993, **99**, 4597; (b) E. van Lenthe, E. J. Baerends and J. G. Snijders, *J. Chem. Phys.*, 1994, **101**, 9783; (c) E. van Lenthe, A. E. Ehlers and E. J. Baerends, *J. Chem. Phys.*, 1999, **110**, 8943.
52 (a) E. van Lenthe and E. J. Baerends, *J. Comput. Chem.*, 2003, **24**, 1142; (b) D. P. Chong, E. van Lenthe, S. J. A. van Gisbergen and E. J. Baerends, *J. Comput. Chem.*, 2004, **25**, 1030; (c) D. P. Chong, *Mol. Phys.*, 2005, **103**, 749.
53 (a) G. te Velde, F. M. Bickelhaupt, E. J. Baerends, C. Fonseca Guerra, S. J. A. van Gisbergen, J. G. Snijders and T. Ziegler, Chemistry with ADF, *J. Comput. Chem.*, 2001, **22**, 931; (b) AMS/ADF 2020.1, SCM, Theoretical Chemistry, Vrije Universiteit, Amsterdam, The Netherlands, http://www.scm.com.
54 Y. Zhao and D. G. Truhlar, *J. Phys. Chem. A*, 2005, **109**, 5656.
55 (a) B. Metz, H. Stoll and M. Dolg, *J. Chem. Phys.*, 2000, **113**, 2563; (b) F. Weigend, F. Furche and R. Ahlrichs, *J. Chem. Phys.*,

2003, **119**, 12753; (c) F. Weigend and R. Ahlrichs, *Phys. Chem. Chem. Phys.*, 2005, **7**, 3297; (d) F. Weigend, *Phys. Chem. Chem. Phys.*, 2006, **8**, 1057.

56 P. Erdmann, J. Leitner, J. Schwarz and L. Greb, *ChemPhysChem,* 2020, **21**, 987.